Reduced models of turbulent transport in helical plasmas including effects of zonal flows and trapped electrons

メタデータ	言語: eng
	出版者:
	公開日: 2021-08-04
	キーワード (Ja):
	キーワード (En):
	作成者: TODA, Shinichiro, NUNAMI, Masanori, SUGAMA, Hideo
	メールアドレス:
	所属:
URL	http://hdl.handle.net/10655/00012619

Reduced models of turbulent transport in helical plasmas including effects of zonal flows and trapped electrons

S. Toda†, M. Nunami and H. Sugama

National Institute for Fusion Science / The Graduate University for Advanced Studies, Toki 509-5292, Gifu, Japan

Using the transport models, the impacts of trapped electrons on zonal flows and the turbulence in the helical field configurations are studied. The effect of the trapped electrons on the characteristic quantities of the linear response for zonal flows is investigated for two different field configurations in the Large Helical Device. The turbulent potential fluctuation, zonal flow potential fluctuation and ion energy transport are quickly predicted by the reduced models for which the linear and nonlinear simulation results are used to determine dimensionless parameters related to turbulent saturation levels and typical zonal flow wavenumbers. The effects of zonal flows on the turbulent transport for the case of the kinetic electron response are much smaller than or comparable to those in adiabatic electron condition for the two different field configurations. It is clarified that the effect of zonal flows on the turbulent transport due to the trapped electrons changes, depending on the field configurations.

1. Introduction

The quantitative prediction of the turbulent transport in toroidal plasmas is one of the most critical issues to be solved for realization of fusion energy (Connor & Wilson 1994; Horton 2017). Recently, a large number of gyrokinetic simulations of the turbulent transport in toroidal plasmas have been performed (Garbet *et al.* 1994; Jenko & Dorland 2001; Candy & Waltz 2003; Watanabe *et al.* 2007; Xanthopoulos *et al.* 2007; Nunami *et al.* 2011; Ishizawa *et al.* 2014). The gyrokinetic simulation results for tokamak (Kotschenreuther *et al.* 1995; Holland *et al.* 2011; Rhodes *et al.* 2011; Nakata *et al.* 2016) and helical (Nunami *et al.* 2012, 2013; Toda *et al.* 2019*b*; Ishizawa *et al.* 2015, 2017) plasmas have been compared with the experimental observation results. Since it is known that zonal flows can regulate the turbulent transport, numerous studies have been done to investigate the efficiency of zonal flows to improve plasma confinement in toroidal devices. In these studies, nonlinear gyrokinetic simulations have been performed to accurately determine the relation between the turbulent transport level and the zonal flow amplitude. However, such nonlinear simulations require a huge computational cost for the parameter scan in wide ranges of magnetic field configurations and plasma equilibrium profiles. To reduce the computational cost, the reduced models are proposed. These reduced models can quickly reproduce the nonlinear simulation results of the turbulent transport coefficients and fluxes from the linear simulation results of the instabilities' growth rates and the zonal flow responses in helical plasmas under the conditions of adiabatic electrons (Nunami *et al.* 2013) and kinetic electrons (Toda *et al.* 2019*a*). The turbulent

† Email address for correspondence: toda@nifs.ac.jp

and the zonal flow potential fluctuations can also be estimated by these models. It is also noted that, in the reduced models, dimensionless parameters related to turbulent saturation levels and zonal flow decay times (Sugama & Watanabe 2006; Ferrando-Margalet *et al.* 2007) are determined using the nonlinear simulation data set. These reduced models are presented for the plasmas in the Large Helical Device (LHD), where the ion temperature gradient (ITG) modes are unstable. To evaluate turbulent particle and heat transport fluxes as well as for treating electromagnetic effects which become important for high-β plasmas, kinetic electrons need to be treated in linear and nonlinear gyrokinetic simulations. In particular, in helical plasmas, trapped electrons show complicated drift motions and it is a serious challenge to quantitatively clarify how they impact instabilities, zonal flows, and turbulent transport.

At first, the reduced model for the ion heat diffusivity is constructed for the cases of both the adiabatic and the kinetic electron responses. The effects of trapped electrons on zonal flows and turbulent transport in the LHD configuration are studied. The residual zonal flow level for the case of kinetic electrons is compared with that in the adiabatic electron condition by the linear gyrokinetic simulation for the plasmas in the LHD, where the ITG mode is unstable. The residual level of zonal flows has been studied in tokamak and helical plasmas by the gyrokinetic simulations (Monreal *et al.* 2016). In addition, the zonal flow decay time for the kinetic electron case is compared with that in the adiabatic electron condition. Next, evaluating the mixing length estimate and the zonal flow decay time by the linear gyrokinetic simulations, the saturation levels of turbulence and zonal flows are predicted from the reduced transport models with setting different field configurations and plasma equilibrium profiles for which effects of electrons on zonal flows and plasma confinement are investigated.

2. Models for turbulence, zonal flows and transport

The turbulence driven by the microinstabilities and zonal flows in the LHD plasmas are studied, using the gyrokinetic local flux tube code, GKV (Watanabe & Sugama 2006). In this section, the diffusivity and quasilinear flux models for the ion heat transport are shown (Nunami *et al.* 2013; Toda *et al.* 2019a) for the adiabatic electron condition and the kinetic electron condition. These reduced models are constructed, where the ITG mode is unstable. The models for the electrostatic turbulent and zonal flow potential fluctuations are also shown. In this article, electrons are treated by two ways. In the first way, for kinetic electron case, the electromagnetic gyrokinetic equation for the electron is solved. In the second simplified way, the electron density perturbation δn_e is given (Nunami *et al.* 2012) in terms of the electrostatic potential fluctuation by

$$\frac{\delta n_{e,\tilde{k}_x,\tilde{k}_y}}{n_0} = \begin{cases} e\left[\tilde{\phi}_{\tilde{k}_x,\tilde{k}_y} - \left\langle \tilde{\phi}_{\tilde{k}_x,\tilde{k}_y} \right\rangle\right]/T_e & \text{if } \tilde{k}_y = 0 \\ e\tilde{\phi}_{\tilde{k}_x,\tilde{k}_y}/T_e & \text{if } \tilde{k}_y \neq 0, \end{cases} \tag{2.1}$$

where e is the elementary charge, n_0 is the background density, T_e is the electron temperature, $\tilde{\phi} = \phi/((T_i/e)(\rho_i/R))$, R is the major radius and $\rho_i(= m_i v_{ti}/(eB))$ is the thermal ion gyroradius. Here, m_i is the ion mass, B is the magnetic field strength, $v_{ti}(= \sqrt{T_i/m_i})$ is the thermal ion velocity and T_i is the ion temperature. The average along the field line is denoted by $\langle \cdots \rangle$ and $\tilde{k}_x(= k_x \rho_i)$ and $\tilde{k}_y(= k_y \rho_i)$ are the normalized radial and poloidal wavenumbers, respectively. Equation (2.1) is called the modified adiabatic electron response, in which the response at $\tilde{k}_y = 0$ is not rigorously the adiabatic electron response. The models for the squared turbulent and zonal flow potential fluctuations,
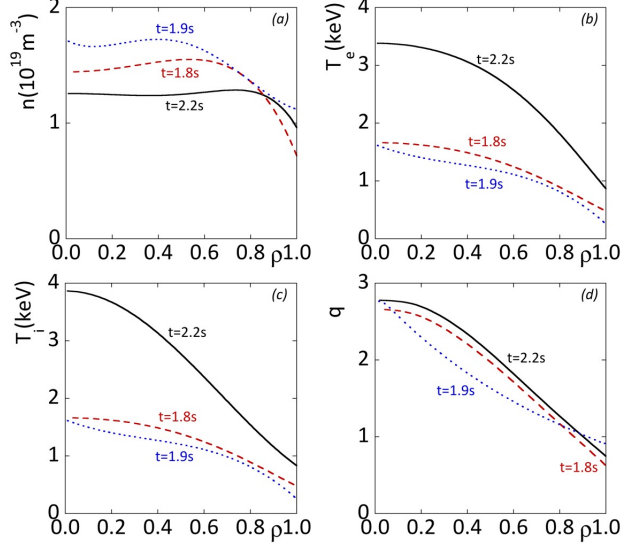
FIGURE 1. The radial profiles of the density (a), the ion (b), the electron (c) temperatures and the safety factor (d) are shown. The solid, dashed and dotted curves represent the profiles at $t = 2.2$s for the standard field configuration, $t = 1.8$s and $t = 1.9$s for the inward-shifted configuration in the LHD #88343 plasmas, respectively.

$\mathcal{T} \left(= \sum_{\tilde{k}_x, \tilde{k}_y \neq 0} \left\langle \left| \tilde{\phi}_{\tilde{k}_x, \tilde{k}_y} \right|^2 \right\rangle / 2 \right)$ and $\mathcal{Z} \left(= \sum_{\tilde{k}_x} \left\langle \left| \tilde{\phi}_{\tilde{k}_x, \tilde{k}_y = 0} \right|^2 \right\rangle / 2 \right)$ are also represented by the linear simulation results, to reproduce the nonlinear simulation results. The models are constructed by using the plasma profiles of the experimental results in the LHD shot number 88343 (Tanaka *et al.* 2010), using the equilibrium field configurations by the VMEC calculations. The major radii of the plasmas are given by $R = 3.75$m for the standard field configuration and $R = 3.6$m for the inward-shifted field configuration. The abbreviations *SD* and *IW* used in this article stand for the standard and inward shifted field configurations, respectively. The profiles of the density n (a), the electron T_e (b) and the ion T_i (c) temperatures are shown in figure 1. The safety factor q profile is also shown in figure 1(d). The solid, dashed and dotted curves represent the profiles at $t = 2.2$s for the SD, $t = 1.8$s and $t = 1.9$s for the IW, respectively. It should be emphasized that the reduced models explained below reproduce the nonlinear simulation results and the reduced models are derived from the simulations by the plasma parameters at the twenty radial points in the radial region $0.46 < \rho < 0.80$ in the two different field configurations, the SD and the IW. The experimentally observed fluctuations in these plasmas are driven by the ITG mode (Nunami *et al.* 2011) and these plasmas are chosen as the representative plasmas for the study of the ITG mode.

The reduced model of the ion heat diffusivity for the adiabatic electron case is introduced. The reduced model in the adiabatic electron condition is derived by the results using the plasma profile at $t = 2.2$s for both the SD and IW. The transport model in terms of $\bar{\mathcal{T}}$ and $\bar{\mathcal{Z}}$ (Nunami *et al.* 2013) is shown by

$$\mathcal{F}_{\text{ad}}(\bar{\mathcal{T}}, \bar{\mathcal{Z}}) = \frac{C_{1,\text{ad}} \bar{\mathcal{T}}^{\alpha_{\text{ad}}}}{C_{2,\text{ad}} + \bar{\mathcal{Z}}^{\frac{1}{2}} / \bar{\mathcal{T}}}, \qquad (2.2)$$

where $\alpha_{\text{ad}} = 0.38$, $C_{1,\text{ad}} = 6.3 \times 10^{-2}$ and $C_{2,\text{ad}} = 1.1 \times 10^{-2}$. Here, the symbol $^-$ denotes the time averaged value in the nonlinear saturation phase. The values of the exponent and

the coefficients are determined when the relative error between the nonlinear simulation result and the transport model is minimized. The models for the electrostatic turbulent and zonal flow potential fluctuations for the adiabatic electron condition (Nunami *et al.* 2013) are given by

$$\bar{\mathcal{T}} = C_{\mathrm{T,ad}}\mathcal{L} \tag{2.3}$$

and

$$\left(\frac{\bar{\bar{\mathcal{Z}}}}{\bar{\bar{\mathcal{T}}}}\right)^{\frac{1}{2}} = C_{\mathrm{Z,ad}}\tilde{\tau}_{\mathrm{ZF}} \tag{2.4}$$

with $C_{\mathrm{T,ad}} = 9.8 \times 10$ and $C_{\mathrm{Z,ad}} = 0.20$. Here, $\mathcal{L}\left(\equiv \int (\tilde{\gamma}_{\tilde{k}_y}/\tilde{k}_y^2)d\tilde{k}_y\right)$ is the quantity related with the mixing length estimate and $\tilde{\gamma}_{\tilde{k}_y}(=\gamma_{\tilde{k}_y}/(v_{ti}/R))$ is the normalized linear growth rate of the ITG mode. The linear zonal flow response function is defined by $\mathcal{R}_{\tilde{k}_x}(t) \equiv \left\langle \tilde{\phi}_{\tilde{k}_x, \tilde{k}_y=0}(t) \right\rangle / \left\langle \tilde{\phi}_{\tilde{k}_x, \tilde{k}_y=0}(t=0) \right\rangle$. Note that the zonal flow response function for $\tilde{k}_x = 0.25$ is used to evaluate the representative values of the zonal flow decay time, because there are peaks of the wavenumber spectra around $\tilde{k}_x = 0.25$ in the nonlinear simulation results. To study the correlation between $\mathcal{R}_{\tilde{k}_x}(t)$ and the fluctuation of zonal flows $\bar{\mathcal{Z}}$, the zonal flow decay time (Sugama & Watanabe 2006; Ferrando-Margalet *et al.* 2007) is employed. The zonal flow decay time is defined by $\tau_{ZF} \equiv \int_0^{\tau_f} dt \mathcal{R}_{\tilde{k}_x}(t)$, where the upper limit τ_f in the integral is set to be $\tau_f = 25R/v_{ti}$ in the modified adiabatic electron condition for modeling the diffusivities or fluxes. The correlation time of the turbulent sources is shorter than $25R/v_{ti}$. Therefore, the zonal flow response function for $\tau_f > 25R/v_{ti}$ is not considered to influence the generated zonal flow level. The normalized zonal flow decay time is defined as $\tilde{\tau}_{ZF} = \tau_{ZF}/(R/v_{ti})$. When the plasma profiles change, the values of $\tilde{k}_x$ and τ_f are determined for the simulation of the linear response for zonal flows from the nonlinear simulation results. It is anticipated that the reduced models predict the nonlinear simulation results for the other ITG plasmas in the LHD than the plasmas used for constructing the reduced models, where the simulation for the linear response of zonal flows is performed at the fixed $\tilde{k}_x$ and τ_f. The helical magnetic structure in the inward-shifted field configuration enhances the zonal flow generation (Watanabe *et al.* 2008). If equations (2.3) and (2.4) are substituted into equation (2.2), the ion heat diffusivity model for the adiabatic electron condition (Nunami *et al.* 2013) is represented by

$$\frac{\chi_{\mathrm{i}}^{\mathrm{model}}}{\chi_{\mathrm{i}}^{\mathrm{GB}}} = \frac{A_{1,\mathrm{ad}}\mathcal{L}^{\alpha_{\mathrm{ad}}}}{A_{2,\mathrm{ad}} + \tilde{\tau}_{\mathrm{ZF}}/\mathcal{L}^{\frac{1}{2}}}, \tag{2.5}$$

where $\chi_{\mathrm{i}}^{\mathrm{GB}}(=\rho_{\mathrm{i}}^2 v_{\mathrm{ti}}/R)$ is the gyro-Bohm diffusivity. The coefficient is given by $A_{1,\mathrm{ad}} = C_{1,\mathrm{ad}}C_{\mathrm{T,ad}}^{\alpha_{\mathrm{ad}}+1/2}C_{\mathrm{Z,ad}}^{-1} = 1.8 \times 10$ and $A_{2,\mathrm{ad}} = C_{2,\mathrm{ad}}C_{\mathrm{T,ad}}^{1/2}C_{\mathrm{Z,ad}}^{-1} = 5.2 \times 10^{-1}$. By use of the reduced model for the modified adiabatic electron condition, the validation study was done for the other plasmas in the LHD than the LHD#88343 plasmas, where the ITG mode is unstable. The ion temperature profile for the simulation results is predicted to be comparable to that for the experimental results (Toda *et al.* 2015).

Next, the reduced model of the ion heat diffusivity for the kinetic electron response is introduced. The reduced model for the kinetic electron response is derived by the results using the plasma profiles at $t = 2.2$s for the SD, and at $t = 1.8$s and $t = 1.9$s for the IW.

The transport model in terms of $\bar{\mathcal{T}}$ and $\bar{\mathcal{Z}}$ (Toda *et al.* 2019*a*) is shown by

$$\mathcal{F}_{\text{ke}}(\bar{\mathcal{T}}, \bar{\mathcal{Z}}) = \frac{C_{1,\text{ke}} \bar{\mathcal{T}}^{\alpha_{\text{ke}}}}{C_{2,\text{ke}} + \bar{\mathcal{Z}}^{\frac{1}{2}}/\bar{\mathcal{T}}}, \tag{2.6}$$

where $\alpha_{\text{ke}} = 0.41$, $C_{1,\text{ke}} = 0.13$ and $C_{2,\text{ke}} = 4.9 \times 10^{-2}$. The models for the electrostatic turbulent and zonal flow potential fluctuations for the case of the kinetic electron response (Toda *et al.* 2019*a*) are represented by

$$\bar{\mathcal{T}} = C_{\text{T,ke}} \mathcal{L}^{a_{\text{ke}}} \tag{2.7}$$

and

$$\frac{\bar{\mathcal{Z}}^{b_{\text{ke}}}}{\bar{\mathcal{T}}^{c_{\text{ke}}}} = C_{\text{Z,ke}} \tilde{\tau}_{\text{ZF}} \tag{2.8}$$

with $C_{\text{T,ke}} = 6.6 \times 10$, $C_{\text{Z,ke}} = 0.19$, $a_{\text{ke}} = 1.6$, $b_{\text{ke}} = 0.16$ and $c_{\text{ke}} = 0.27$. The upper limit τ_f in the integral is set to be $\tau_f = 30R/v_{\text{ti}}$ in the kinetic electron condition, which is larger than that ($\tau_f = 25R/v_{\text{ti}}$) in the adiabatic electron condition. Even if the reduced models for the kinetic electron response are constructed for $\tau_f = 25R/v_{\text{ti}}$, the values of the coefficients and the exponents in the reduced models nearly unchanged. The ion heat diffusivity model for the case of the kinetic electron response (Toda *et al.* 2019*a*) is shown by

$$\frac{\chi_{\text{i}}^{\text{model}}}{\chi_{\text{i}}^{\text{GB}}} = \frac{A_{1,\text{ke}} \mathcal{L}^{B_1}}{A_{2,\text{ke}} + \tilde{\tau}_{\text{ZF}}^{B_2}/\mathcal{L}^{B_3}}, \tag{2.9}$$

where $A_{1,\text{ke}} = C_{1,\text{ke}} C_{\text{T,ke}}^{\alpha_{\text{ke}}+1-c_{\text{ke}}/(2b_{\text{ke}})} C_{\text{Z,ke}}^{-1/(2b_{\text{ke}})} = 2.6 \times 10^2$ and $A_{2,\text{ke}} = C_{2,\text{ke}} C_{\text{T,ke}}^{1-c_{\text{ke}}/(2b_{\text{ke}})} C_{\text{Z,ke}}^{-1/(2b_{\text{ke}})} = 1.8 \times 10$. The exponents are given by $B_1 = a_{\text{ke}} \alpha_{\text{ke}} = 3.1$, $B_2 = 1/(2b_{\text{ke}}) = 0.26$ and $B_3 = a_{\text{ke}}(1 - c_{\text{ke}}/(2b_{\text{ke}})) = 0.26$. The quasilinear flux model of the ion heat transport for the case of the kinetic electron response (Toda *et al.* 2019*a*) is shown as

$$\tilde{Q}_{\text{i,ql}}^{\text{model}} = C_{Q_{\text{i}}} \int \frac{\tilde{Q}_{\text{i},\tilde{k}_y}^{\text{lin}}}{\left\langle |\tilde{\phi}_{\tilde{k}_y}^{\text{lin}}|^2 \right\rangle} \left\langle |\tilde{\phi}_{\tilde{k}_y}|^2 \right\rangle^{\text{model}} d\tilde{k}_y, \tag{2.10}$$

where the quantities with the superscript "lin" represent the linear simulation results. Here, the tilde ˜ represents the normalization of the ion energy flux by the values of $nT_{\text{i}}v_{\text{ti}}\rho_{\text{i}}^2/R^2$. The ion energy flux is $Q_{\text{i}}(= Q_{\text{i}}^{\text{es}} + Q_{\text{i}}^{\text{em}})$, where the electrostatic part is $Q_{\text{i}}^{\text{es}} = Re \left\langle \sum_{\boldsymbol{k}_\perp} \int (m_{\text{i}} v_\parallel^2 + \mu_0 B) h_{\text{i}\boldsymbol{k}_\perp} J_{0i} d^3 v (-\mathrm{i} k_y \phi_{\boldsymbol{k}_\perp}/B)^*/2 \right\rangle_f$ and the electromagnetic part is $Q_{\text{i}}^{\text{em}} = Re \left\langle \sum_{\boldsymbol{k}_\perp} \int v_{\text{ti}} v_\parallel (m_{\text{i}} v_\parallel^2 + \mu_0 B) h_{\text{i}\boldsymbol{k}_\perp} J_{0j} d^3 v (\mathrm{i} k_y A_{\parallel \boldsymbol{k}_\perp}/B)^*/2 \right\rangle_f$ (Ishizawa *et al.* 2015). The symbol $< \cdots >_f$ represents the flux surface average. Here, $v_\parallel$, μ_0, v, ϕ and $A_{\parallel \boldsymbol{k}_\perp}$ are the parallel velocity, the permeability in vacuum, the velocity, the electrostatic potential and the electromagnetic potential, respectively. The term $h_{\text{i}\boldsymbol{k}_\perp}$ represents the non-adiabatic part of the perturbed part in the gyro-center distribution function, $J_{0i}(= J_0(\rho_i k_\perp))$ is the zeroth order Bessel function and $\boldsymbol{k}_\perp = (k_x, k_y)$. The values of $\tilde{\gamma}_{\tilde{k}_y}$, $\tilde{Q}_{\text{i},\tilde{k}_y}^{\text{lin}}$ and $\left\langle |\tilde{\phi}_{\tilde{k}_y}^{\text{lin}}|^2 \right\rangle$ are estimated by the linear simulation with $\tilde{k}_x = 0$, where the plasma is considered to be most unstable. In the linear simulation, the flux and potential fluctuation grow exponentially, but the ratio of the two becomes constant. The coefficient $C_{Q_{\text{i}}}$ is given by 0.58. The quasilinear flux is proportional to the product of the linear response function and the nonlinear electrostatic potential fluctuation. The model

function with the mixing length estimate and the zonal flow decay time is represented as

$$\left\langle |\tilde{\phi}_{\tilde{k}_y}|^2 \right\rangle^{\text{model}} = \frac{C_{\text{q1}}(\tilde{\gamma}_{\tilde{k}_y}/\tilde{k}_y^2)^{\alpha_{\text{q1}}}}{C_{\text{q2}} + \tilde{\tau}_{\text{ZF}}^{\alpha_{\text{ZF}}}/(\tilde{\gamma}_{\tilde{k}_y}/\tilde{k}_y^2)^{\alpha_{\text{q2}}}}. \tag{2.11}$$

The parameters are determined as $C_{\text{q1}} = 1.0 \times 10^2$, $C_{\text{q2}} = 9.2 \times 10^{-4}$, $\alpha_{\text{q1}} = 0.54$, $\alpha_{\text{q2}} = 0.12$ and $\alpha_{\text{ZF}} = 1.6$. For the ion heat transport, the linear simulation results of the quantity related with the mixing length estimate and the zonal flow decay time reproduce the nonlinear simulation result by the quasilinear flux model. Capturing the dependence of the turbulent transport on the linear properties, the formula for the reduced models shown above can be applied to tokamak plasmas (Nakata *et al.* 2014), by adjusting the coefficients and the exponents in the reduced models.

3. Reduced model of ion heat diffusivity both for modified adiabatic and kinetic electron conditions

The two different reduced models for the cases of the modified adiabatic electron (MAE) and kinetic electron (KE) responses were already proposed (Nunami *et al.* 2013; Toda *et al.* 2019*a*) and explained in §2. If the ion heat diffusivity both for the cases of the MAE and KE responses are approximated by one reduced model, the relative error is evaluated for reproducing the nonlinear simulation results by the reduced model. Note that the different dependences on the turbulent potential fluctuation, $\bar{\mathcal{T}}$ and the zonal flow potential fluctuation, $\bar{\mathcal{Z}}$ are predicted for the cases of the MAE and the KE responses. The model function for the ion heat diffusivity as the function of $\bar{\mathcal{T}}$ and $\bar{\mathcal{Z}}$ is shown as

$$\mathcal{F}(\bar{\mathcal{T}}, \bar{\mathcal{Z}}) = \frac{C_1 \bar{\mathcal{T}}^{\alpha}}{C_2 + \bar{\mathcal{Z}}^{\xi}/\bar{\mathcal{T}}}. \tag{3.1}$$

The nonlinear simulation results for $\chi_i/\chi_i^{\text{GB}}$ are fitted by the model function (3.1) using the twenty data for the case of the KE response and the twenty-one data for the case of the MAE response. The twenty fit points for the MAE condition in the SD and IW are the simulation results for the plasmas at $t = 2.2$s for LHD shot number 88343. The ten fit points for the KE response in the SD are the simulation results for the plasmas at $t = 2.2$s. The ten fit points for the KE response in the IW are the simulation results for the plasmas at $t = 1.8, 1.9$s. When the relative errors are minimized between the nonlinear simulation results and the model function, the fitting parameters are determined as $C_1 = 0.079$, $C_2 = 0.015$, $\alpha = 0.38$ and $\xi = 0.55$. Figure 2 shows the comparison of the nonlinear simulation results, $\bar{\chi}_i/\chi_i^{\text{GB}}$ with the model function (3.1). The circle and square marks correspond to the cases for the MAE and KE conditions, respectively. The relative error for fitting the nonlinear simulation results, $\bar{\chi}_i/\chi_i^{\text{GB}}$ by $\mathcal{F}(\bar{\mathcal{T}}, \bar{\mathcal{Z}})$ is $\sigma = 0.30$, where σ is $\sqrt{\sum \left(\bar{\chi}_i/(\chi_i^{\text{GB}}\mathcal{F}) - 1 \right)^2 / 41}$. The relative error (0.30) becomes larger than that only by the MAE (0.15) or KE condition (0.16).

Using both sets of data for the cases of the KE and MAE responses, the turbulent electrostatic potential fluctuation $\bar{\mathcal{T}}$ is approximated as $\bar{\mathcal{T}} = C_{\text{T}}\mathcal{L}^a$, where $C_{\text{T}} = 7.2 \times 10$ and $a = 1.5$. The zonal flow electrostatic potential fluctuation $\bar{\mathcal{Z}}$ is also approximated by the relation $\tilde{\tau}_{\text{ZF}} = C_{\text{Z}}\bar{\mathcal{Z}}^b/\bar{\mathcal{T}}^c$, where $C_{\text{Z}} = 0.22$, $b = 0.16$ and $c = 0.24$. When the equation (3.1) is rewritten by the linear simulation results for $\bar{\mathcal{T}}$ and $\bar{\mathcal{Z}}$, the ion heat
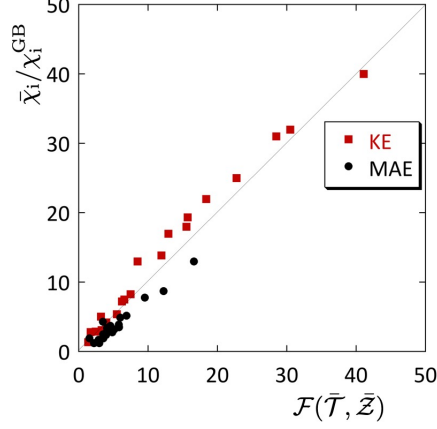
FIGURE 2. The nonlinear simulation results, $\bar{\chi}_i/\chi_i^{\mathrm{GB}}$ are compared with the model function (3.1). The circle and square marks correspond to the cases for the modified adiabatic electron (MAE) and kinetic electron (KE) conditions, respectively.
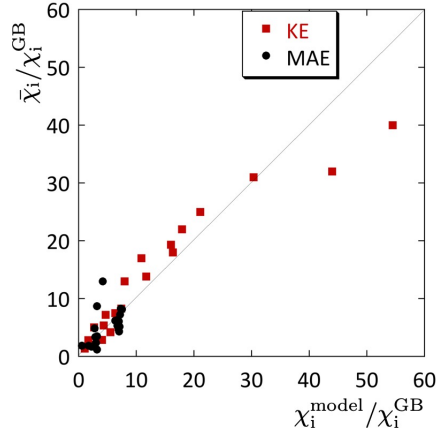

FIGURE 3. The comparison of the nonlinear simulation results, $\bar{\chi}_i/\chi_i^{\mathrm{GB}}$ with the reduced model (3.2) is shown. The circle and square marks correspond to the cases for the modified adiabatic electron (MAE) and kinetic electron (KE) conditions, respectively.

diffusivity model is represented in terms of $\mathcal{L}$ and $\tilde{\tau}_{\mathrm{ZF}}$, as

$$\frac{\bar{\chi}_i^{\mathrm{model}}}{\chi_i^{\mathrm{GB}}} = \frac{A_1 \mathcal{L}^{B_1}}{A_2 + \tilde{\tau}_{\mathrm{ZF}}^{B_2}/\mathcal{L}^{B_3}}, \tag{3.2}$$

where the coefficients are given by $A_1 = C_1 C_T^{\alpha+1-c\xi/b} C_Z^{-\xi/b} = 1.5 \times 10^2$ and $A_2 = C_2 C_T^{1-c\xi/b} C_Z^{-\xi/b} = 5.6$. The exponents are given by $B_1 = a\alpha = 0.57$, $B_2 = \xi/b = 3.4$ and $B_3 = a(1-c\xi/b) = 0.27$. The normalized ion heat diffusivity, $\bar{\chi}_i/\chi_i^{\mathrm{GB}}$ obtained from the nonlinear simulation is compared with the model prediction $\chi_i^{\mathrm{model}}/\chi_i^{\mathrm{GB}}$ in figure 3, where the circles and boxes show the results for the cases of the MAE and KE responses, respectively. When using the definition of the root mean square error (Kinsey *et al.* 2008) $\sqrt{\sum(\bar{\chi}_i/\chi_i^{\mathrm{GB}} - \chi_i^{\mathrm{model}}/\chi_i^{\mathrm{GB}})^2 / \sum(\chi_i^{\mathrm{model}}/\chi_i^{\mathrm{GB}})^2}$, its value is as small as 0.27.

4. Linear simulation results for zonal flows

In this section, the linear simulation results related with zonal flows for the MAE condition of (2.1) are compared with those for the case of the KE response in the SD and IW. In this analysis, the collision frequency for the plasmas at $t = 2.2$s is used for the analysis in the SD and the IW. When the field configuration model was used, it was analytically shown that the linear response function decays faster due to the presence of the trapped particles than for the MAE condition. It was found that the residual level for zonal flows complicatedly depends on the helical ripple and the ratio of the neoclassical polarization due to toroidally trapped particles to the classical polarization (Sugama & Watanabe 2006). Figure 4 shows the linear response of zonal flows at $\tilde{k}_x = 0.25$, $\mathcal{R}_{\tilde{k}_x=0.25}(t)$ at $\rho = 0.65$ in the SD (a) and IW (b). The solid and dashed curves represent the cases for the MAE and KE conditions, respectively. The linear zonal flow response function for the case of the KE response is confirmed to decay faster than that for the MAE response in the SD and IW. The residual level of zonal flows for the case of the KE response is smaller than that for the MAE response in the SD at $\rho = 0.65$. This tendency is the same in the SD at $\rho = 0.80$ (Toda *et al.* 2017). However, it is clarified that the residual level for the KE condition is found to be closer to that for the MAE condition at $\rho = 0.65$ in the IW in figure 4(b) than in the SD. Figure 5 shows the radial dependences of the zonal flow decay time, $\tilde{\tau}_{\mathrm{ZF}}$ on the radial position in the SD and IW. For comparing the zonal flow decay time for the case of the KE response with that for the MAE condition, the value of τ_f is set to be $30R/v_{\mathrm{ti}}$ for the MAE and KE conditions. The zonal flow decay time is larger for the MAE condition than for the KE condition in the SD and the IW in figure 5. The zonal flow decay times in the IW for the MAE and KE conditions are found to be larger than those in the SD for the MAE and KE conditions, respectively. Radial drift motion of kinetic electrons is considered to relax the potential difference in the radial direction and accordingly weaken zonal flows (Sugama & Watanabe 2006). For larger ρ, fractions of trapped electrons increase and further reduction of zonal flows occurs as shown in figure 5. The difference of the magnitude relationship of the residual level for zonal flows or the zonal flow decay time in the SD and IW is due to the complicated dependence on the helical ripple and the effect of the toroidally trapped particles. Figure 6 shows the ratio of the zonal flow decay time for the KE response, $\tilde{\tau}_{\mathrm{ZF}}(KE)$ to that for the MAE condition, $\tilde{\tau}_{\mathrm{ZF}}(MAE)$. It is found that the ratio $\tilde{\tau}_{\mathrm{ZF}}(KE)/\tilde{\tau}_{\mathrm{ZF}}(MAE)$ in the IW is larger than that in SD. The incline of zonal flows due to kinetic electrons is reduced in the IW, where the radial drift of kinetic electrons slows down.

5. Model predictions for the nonlinear simulation results

In this section, the nonlinear simulation results, such as the ion heat diffusivity, χ_{i} as well as the turbulent and the zonal flow potential fluctuations, $\bar{\mathcal{T}}$ and $\bar{\mathcal{Z}}$, are reproduced and predicted by the models explained in § 2. The model reproductions and predictions for the case of the KE response are compared with those for the adiabatic electron (AE) condition. In this article, the difference between the simulations in the SD and the IW is only the field configuration. The plasma parameters at $t = 2.2$s in the shot number #88343 for the LHD, such as the gradients, are used for the reduced models and the nonlinear simulation for both the SD and the IW, to compare with the simulation results for the SD and IW. The simulation results for the KE response in the IW are the true "model prediction", because the plasma parameters at $t = 2.2$s in figure 1 are out of the range on which the models (2.9) and (2.10) are constructed. On the other hand, the
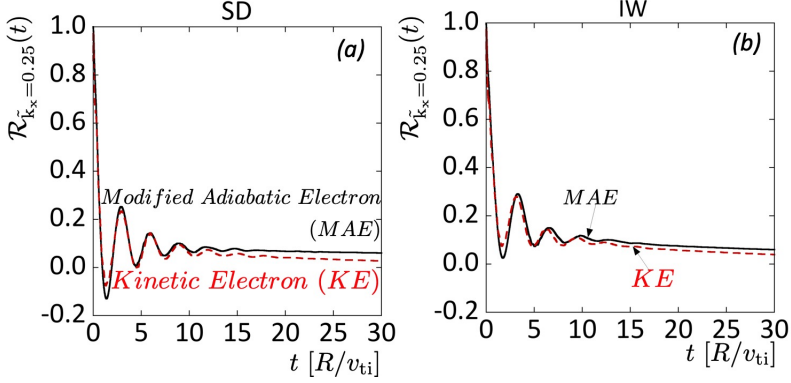
FIGURE 4. The linear responses of zonal flows at $\tilde{k}_x = 0.25$ are shown for (a) the standard field configuration (SD) and (b) the inward-shifted field configuration (IW) at $\rho = 0.65$. The black and red curves represent the linear responses of zonal flows for the cases of the modified adiabatic (MAE) and the kinetic electron (KE) responses, respectively.
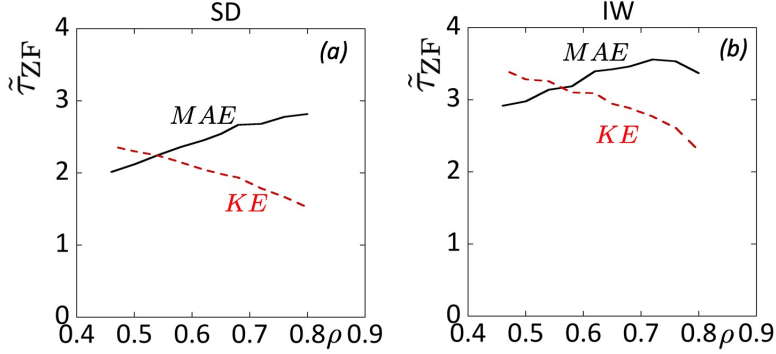

FIGURE 5. The radial dependences of the zonal flow decay time, $\tilde{\tau}_{ZF}$ are shown for (a) the standard field configuration (SD) and (b) the inward-shifted field configuration (IW). The black and red curves represent the radial dependences of $\tilde{\tau}_{ZF}$ for the cases of the modified adiabatic (MAE) and kinetic electron (KE) responses, respectively.
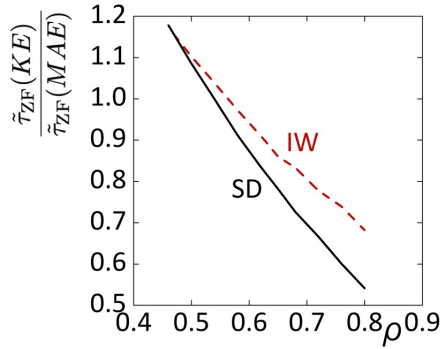
FIGURE 6. The radial dependences of the ratio $\tilde{\tau}_{ZF}(KE)/\tilde{\tau}_{ZF}(MAE)$ are shown for the standard field configuration (SD) and the inward-shifted field configuration (IW), where $\tilde{\tau}_{ZF}(MAE)$ and $\tilde{\tau}_{ZF}(KE)$ are the zonal flow decay times for the modified adiabatic (MAE) and kinetic electron (KE) responses, respectively. The black and red curves represent the radial dependences of $\tilde{\tau}_{ZF}(KE)/\tilde{\tau}_{ZF}(MAE)$ for the SD and IW configurations, respectively.
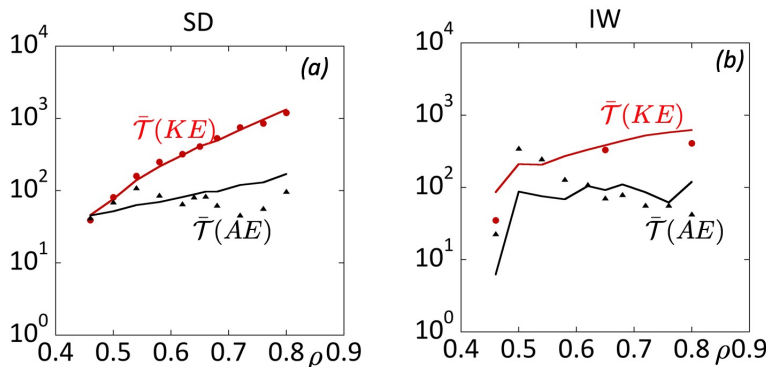
FIGURE 7. The radial dependence of the model reproductions and predictions for the turbulent potential fluctuation, $\bar{\mathcal{T}}$ is shown for (*a*) the standard field configuration (SD) and (*b*) the inward-shifted field configuration (IW). The black and red curves represent the model predictions for $\bar{\mathcal{T}}$ in the adiabatic (AE) and kinetic electron (KE) conditions, respectively. The circle and triangle marks indicate the nonlinear simulation results of $\bar{\mathcal{T}}$ for the KE and AE conditions, respectively.

simulation results for the MAE condition in the SD and the IW, and for the KE response in the SD are the model reproductions for the nonlinear simulation results, which are used for constructing the reduced model. Figure 7 shows the radial dependences of the turbulent potential fluctuation, $\bar{\mathcal{T}}$ in the SD (a) and the IW (b). The red and black curves represent the model reproductions and predictions by (2.3) and (2.7) using the linear simulation results, $\mathcal{L}$ and $\tilde{\tau}_{\mathrm{ZF}}$ for the KE and AE conditions, respectively. The circle and triangle marks indicate the nonlinear simulation results of $\bar{\mathcal{T}}$ for the KE and AE conditions, respectively. The values of $\bar{\mathcal{T}}$ for the case of the KE response are found to be larger than those for the AE condition in both field configurations, because the trapped electron enhances the growth rate of the ITG. Turbulence potential fluctuations in the IW are close to that in the SD in figure 7. The models can reproduce and predict the nonlinear simulation results for $\bar{\mathcal{T}}$, except for the region $\rho < 0.6$ in the IW. Figure 8 shows the radial dependences of the zonal flow potential fluctuation, $\bar{\mathcal{Z}}$ reproduced and predicted by (2.4) and (2.8) in the SD (a) and the IW (b). The zonal flow potential fluctuation, $\bar{\mathcal{Z}}$ in the IW is found to become larger than that in the SD, especially for the case of the KE response. The simulation result confirms that zonal flow potential fluctuation in the IW is larger than that in the SD (Watanabe *et al.* 2008). The model for $\bar{\mathcal{Z}}$ reproduces the nonlinear simulation results in the SD. The model can predict the nonlinear simulation results for the case of the KE response in the IW at $\rho = 0.80$. On the other hand, at $\rho = 0.65$ for the KE response in the IW, the value of $\bar{\mathcal{Z}}$ predicted by the model is significantly larger than the nonlinear simulation result although the model qualitatively explains the tendency of change in $\bar{\mathcal{Z}}$ due to the KE effect. It is still necessary to quantitatively improve the predictability using the extended nonlinear data set for modifying the model parameters.

Figure 9 indicates the radial dependences of $\chi_i^{\mathrm{model}}/\chi_i^{\mathrm{GB}}$ by (2.5) and (2.9) with the solid curve and that for $\bar{\mathcal{Z}} = 0$ with the dashed curve in the SD (a) and the IW (b). The difference between the dashed and solid curves represents the zonal flow effect. In the SD, the zonal flow effect is stronger for the the MAE condition than for the KE condition. On the other hand, in the IW, the zonal effect for the case of the KE response is comparable to that for the MAE condition. When the results in the SD and IW are compared, the zonal flow effect is comparable to that for the MAE condition. On the
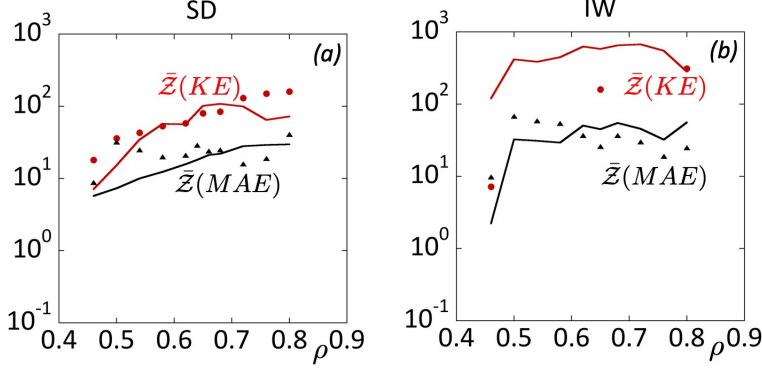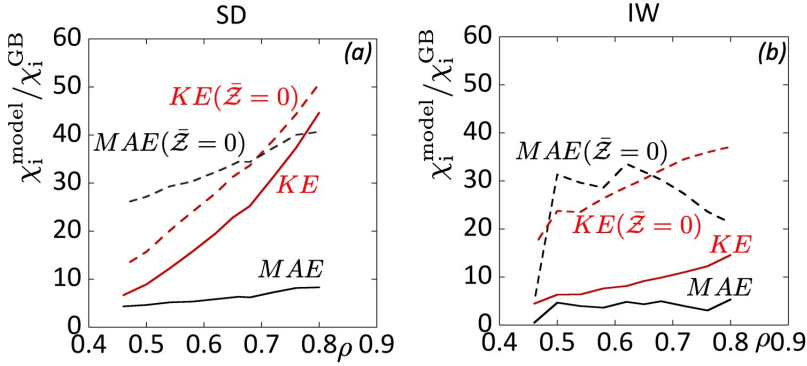
FIGURE 8. The radial dependence of the model reproductions and predictions for the zonal flow potential fluctuation, $\bar{\mathcal{Z}}$ is shown for (a) the standard field configuration (SD) and (b) the inward-shifted field configuration (IW). The black and red curves represent the model predictions for $\bar{\mathcal{Z}}$ for the modified adiabatic (MAE) and kinetic electron (KE) conditions, respectively. The circle and triangle marks indicate the nonlinear simulation results of $\bar{\mathcal{Z}}$ for the KE and MAE conditions, respectively.

FIGURE 9. The radial dependences of the normalized ion heat diffusivity, $\chi_i^{\mathrm{model}}/\chi_i^{\mathrm{GB}}$ (the solid curve) and that for $\bar{\mathcal{Z}} = 0$ (the dashed curve) are shown for (a) the standard field configuration (SD) and (b) the inward-shifted field configuration (IW). The black and red curves represent the model predictions for $\chi_i/\chi_i^{\mathrm{GB}}$ for the cases of the modified adiabatic (MAE) and kinetic electron (KE) responses, respectively.

other hand, the zonal flow effect in the IW is much stronger than that in the SD for the KE response, because trapped electrons in the IW are predicted to be confined better than in the SD. The linear simulation results $\tilde{\tau}_{\mathrm{ZF}}$ in §3 are qualitatively reflected in these nonlinear simulation results for the zonal effect. Figure 10 represents the radial dependence of the normalized ion heat diffusivity by the ion heat diffusivity model (the red curve) by (2.9), and the quasilinear flux model for the ion heat transport (the blue curve) by (2.10) for the case of the kinetic electron response in the SD (a) and the IW (b). The radial dependence of $\chi_i^{\mathrm{model}}/\chi_i^{\mathrm{GB}}$ is also shown by the ion heat diffusivity model (the black curve), (2.5) for the MAE condition. The circle and triangle marks indicate the nonlinear simulation results of the ion heat diffusivity for the KE and MAE conditions, respectively. The ion diffusivity for the KE condition is found to be larger than that for the MAE condition due to the effect of the trapped electrons. In the IW, the ion diffusivity for the KE condition becomes closer to that for the MAE condition than in the SD. It is clarified that the reduced models reproduce the nonlinear simulation results.
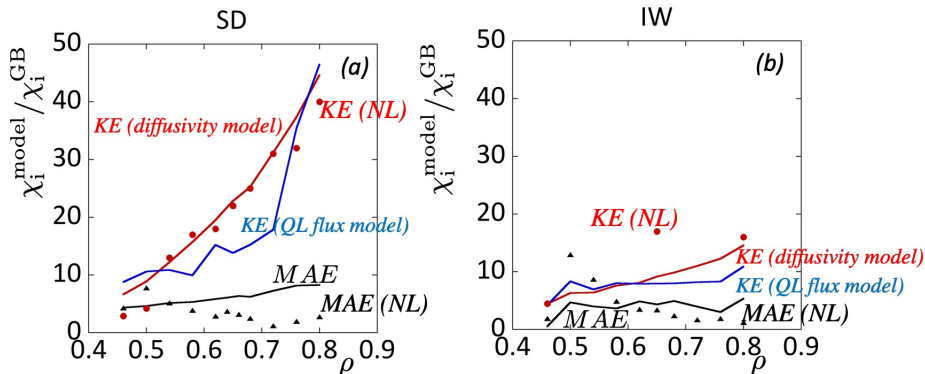
FIGURE 10. The radial dependence of the normalized ion heat diffusivity, χ_i/χ_i^{GB} is shown by the ion heat diffusivity model (the red curve) and the quasilinear flux model for the ion heat transport (the blue curve) for the case of the kinetic electron (KE) response in (*a*) the standard field configuration (SD) and (*b*) the inward-shifted field configuration (IW). The radial dependence of $\chi_i^{model}/\chi_i^{GB}$ is also shown by the ion heat diffusivity model (the black curve) for the modified adiabatic electron (MAE) condition. The circle and triangle marks indicate the nonlinear simulation results of $\chi_i^{model}/\chi_i^{GB}$ in the KE and MAE conditions, respectively.

Even if the linear and nonlinear simulation results in the IW using the plasma profiles at $t = 2.2$s were not adapted for constructing the reduced models for the case of the KE response, the reduced model can predict the nonlinear simulation results in the IW for the case of the KE response. In figure 10, it is found that the transport reproduced and predicted by the reduced models in the IW is smaller than that in the SD.

6. Summary

Effects of trapped electrons on zonal flows and turbulent transport in two kinds of LHD field configurations are studied for the representative plasmas, where the ITG mode is unstable. For the linear simulation results, the residual level and the decay time of zonal flows for the case of the kinetic electron response is smaller than for the modified adiabatic electron response in the SD field configuration. However, the residual level and the decay time of zonal flows for the case of the kinetic electron response are found to become close to those for the modified adiabatic electron response in the IW shifted field configuration. By the reduced models, the zonal flow effect on the transport for the case of the kinetic electron response is weaker than that for the adiabatic electron response in the SD field configuration. In the IW shifted configuration, the zonal flow effect for the case of the kinetic electron response is found to be comparable to that for the adiabatic electron response. The zonal flow effect on the transport depends on not only the zonal flow decay time but also the mixing length estimate in the reduced models. The ion heat diffusivities by the reduced model in the IW shifted field configuration are smaller than those in the SD field configuration. It is found that the linear simulation result, such as the zonal flow decay time, is the possible qualitative criterion for zonal flow effect on the transport. The nonlinear simulation results are well reproduced by the reduced models for the heat diffusivity and the quasilinear flux model in the modified adiabatic condition in the SD and IW, and for the kinetic electron response in the SD. Furthermore, the nonlinear simulation results are predicted by the reduced models for the ion heat transport for the case of the kinetic electron response in the IW, for the plasma parameters, which are out of range for constructing the reduced models. The relative error

for reproducing the nonlinear simulation results by the reduced model is shown when the reduced model for ion heat diffusivity is constructed using the linear and nonlinear simulation results both for the cases of the kinetic and modified adiabatic electron responses. How to construct the model by the linear simulation results (Nunami *et al.* 2013; Toda *et al.* 2019*a*) is applicable by adjusting the coefficients and the exponents in the reduced models and modifying the values of $\tilde{k}_x$ and τ_f for the simulation for the linear response of zonal flows to the other plasmas in helical devices, where other modes than the ITG modes are unstable, and the plasmas in tokamak devices. In helical plasmas, the reduced models for the heat diffusivities have been installed to the transport code, such as TASK3D when the term $\mathcal{L}$ related with the mixing length estimate is modeled by the ion temperature gradient at the dynamically fixed magnetic field, *i.e.*, using the dynamically fixed $\tilde{\tau}_{\rm ZF}$ profile (Toda *et al.* 2019*b*, 2014). In tokamak plasmas, the one-dimensional transport simulation, which is directly coupled to local gyrokinetic analyses, is performed (Candy *et al.* 2009; Barnes *et al.* 2010). To reproduce the nonlinear gyrokinetic simulation results in helical plasmas, the transport simulation directly coupled to the linear gyrokinetic simulation by the reduced models, especially the quasilinear flux models, will be performed. This is for future study.

REFERENCES

BARNES, M., ABEL, I. G., DORLAND, W., GÖRLER, T., HAMMETT, G. W. & JENKO, F. 2010 Direct multiscale coupling of a transport code to gyrokinetic turbulence codes. *Phys. Plasmas* **17**, 056109.

CANDY, J., HOLLAND, C., WALTZ, R. E., FAHEY, M. R. & BELLI, E. 2009 Tokamak profile prediction using direct gyrokinetic and neoclassical simulation. *Phys. Plasmas* **16**, 060704.

CANDY, J. & WALTZ, R. E. 2003 An eulerian gyrokinetic-maxwell solver. *J. Comput. Phys.* **186**, 545.

CONNOR, J. W. & WILSON, H. R. 1994 Survey of theories of anomalous transport. *Plasma Phys. Control. Fusion* **36**, 719.

FERRANDO-MARGALET, S., SUGAMA, H. & WATANABE, T.-H. 2007 Zonal flows and ion temperature gradient instabilities in multiple-helicity magnetic fields. *Phys. Plasmas* **14**, 122505.

GARBET, X., IDOMURA, Y., VILLARD, L. & WATANABE, T.-H. 1994 Gyrokinetic simulations of turbulent transport. *Plasma Phys. Control. Fusion* **36**, 719.

HOLLAND, C., SCHMITZ, L., RHODES, T. L., PEEBLES, W. A., HILLESHEIM, J. C., WANG, G., ZENG, L., DOYLE, E. J., SMITH, S. P., PRATER, R., BURRELL, K. H., CANDY, J., WALTZ, R. E., KINSEY, J. E., STAEBLER, G. M., DEBOO, J. C., PETTY, C. C., MCKEE, G. R., YAN, Z. & WHITE, A. E. 2011 Advances in validating gyrokinetic turbulence models against L- and H-mode plasmas. *Phys. Plasmas* **18**, 056113.

HORTON, W. 2017 *Turbulence Transport in Magnetized Plasmas, 2nd ed.*. World Scientific Pub. Co Inc.

ISHIZAWA, A., KISHIMOTO, Y., WATANABE, T.-H., SUGAMA, H., TANAKA, K., SATAKE,

S., KOBAYASHI, A., NAGASAKI, K. & NAKAMURA, Y. 2017 Multi-machine analysis of turbulent transport in helical systems via gyrokinetic simulation. *Nucl. Fusion* **57**, 066010.

ISHIZAWA, A., WATANABE, T.-H., SUGAMA, H., MAEYAMA, S. & NAKAJIMA, N. 2014 Electromagnetic gyrokinetic turbulence in finite-beta helical plasmas. *Phys. Plasmas* **21**, 055905.

ISHIZAWA, A., WATANABE, T.-H., SUGAMA, H., NUNAMI, M., TANAKA, K., MAEYAMA, S. & NAKAJIMA, N. 2015 Turbulent transport of heat and particles in a high ion temperature discharge of the Large Helical Device. *Phys. Plasmas* **55**, 043024.

JENKO, F. & DORLAND, W. 2001 Nonlinear electromagnetic gyrokinetic simulations of tokamak plasmas. *Plasma Phys. Control. Fusion* **43**, A141.

KINSEY, J. E., STAEBLER, G. M. & WALTZ, R. E. 2008 The first transport code simulations using the trapped gyro-Landau-fluid model. *Phys. Plasmas* **15**, 055908.

KOTSCHENREUTHER, M., DORLAND, W., BEER, M. A. & HAMMET, G. W. 1995 Quantitative predictions of tokamak energy confinement from first principles simulations with kinetic effects. *Phys. Plasmas* **2**, 2381.

MONREAL, P., CALVO, I., SÁNCHEZ, E., PARRA, F., BUSTOS, A., KÖNIES, A., KLEIBER, R. & GÖRLER, T. 2016 Residual zonal flows in tokamaks and stellarators at arbitrary wavelengths. *Plasma Phys. Control. Fusion* **58**, 045018.

NAKATA, M., HONDA, M., YOSHIDA, M., URANO, H., MAEYAMA, S., NUNAMI, M. & WATANABE, T.-H. 2014 Gyrokinetic analysis of turbulent heat and particle transport on JT-60U plasmas. *25th IAEA Fusion Energy Conference St. Petersburg, Russian Federation October 13–18,* TH/P7-34 .

NAKATA, M., HONDA, M., YOSHIDA, M., URANO, H., NUNAMI, M., MAEYAMA, S., WATANABE, T.-H. & SUGAMA, H. 2016 Validation studies of gyrokinetic ITG and TEM turbulence simulations in a JT-60U tokamak using multiple flux matching. *Nucl. Fusion* **56**, 086010.

NUNAMI, M., WATANABE, T.-H. & SUGAMA, H. 2013 A reduced model for ion temperature gradient turbulent transport in helical plasmas. *Phys. Plasmas* **20**, 092307.

NUNAMI, M., WATANABE, T.-H., SUGAMA, H. & TANAKA, K. 2011 Linear gyrokinetic analyses of ITG modes and zonal flows in lhd with high ion temperature. *Plasma Fusion Res.* **6**, 1403001.

NUNAMI, M., WATANABE, T.-H., SUGAMA, H. & TANAKA, K. 2012 Gyrokinetic turbulent transport simulation of a high ion temperature plasma in large helical device experiment. *Phys. Plasmas* **19**, 042504.

RHODES, T. L., HOLLAND, C., SMITH, S. P., WHITE, A. E., BURRELL, K. H., CANDY, J., DEBOO, J. C., DOYLE, E. J., HILLESHEIM, J. C., KINSEY, J. E., MCKEE, G. R., MIKKELSEN, D., PEEBLES, W. A., PETTY, C. C., PRATER, R., PARKER, S., CHEN, Y., SCHMITZ, L., STAEBLER, G. M., WALTZ, R. E., WANG, G., YAN, Z. & ZENG, L. 2011 L-mode validation studies of gyrokinetic turbulence simulations via multiscale and multifield turbulence measurements on the DIII-D tokamak. *Nucl. Fusion* **51**, 063022.

SUGAMA, H. & WATANABE, T.-H. 2006 Collisionless damping of zonal flows in helical systems. *Phys. Plasmas* **13**, 012501.

TANAKA, K., MICHEAL, C., VYACHESLAVOV, L., FUNABA, H., YOKOYAMA, M., IDA, K., YOSHINUMA, M., NAGAOKA, K., MURAKAMI, S., WAKASA, A., IDO, T., SHIMIZU, A., NISHIURA, M., TAKEIRI, Y., KANEKO, O., TSUMORI, K., IKEDA, K., OSAKABE, M., KAWAHATA, K. & GROUP, L. E. 2010 Turbulence response in the high T_i discharge of the LHD. *Plasma and Fusion Research* **5**, S2053.

TODA, S., NAKATA, M., NUNAMI, M., ISHIZAWA, A., WATANABE, T.-H. & SUGAMA, H. 2017 A reduced transport model for ion heat diffusivity by gyro-kinetic analysis with kinetic electrons in helical plasmas. *Plasma and Fusion Research* **12**, 1303035.

TODA, S., NAKATA, M., NUNAMI, M., ISHIZAWA, A., WATANABE, T.-H. & SUGAMA, H. 2019*a* Modeling of turbulent particle and heat transport in helical plasmas based on gyrokinetic analysis. *Phys. Plasmas* **26**, 012510.

TODA, S., NAKATA, M., NUNAMI, M., ISHIZAWA, A., WATANABE, T.-H. & SUGAMA, H. 2019*b* Transport simulation for helical plasmas by use of gyrokinetic transport model. *Plasma and Fusion Research* **14**, 3403061.

TODA, S., NUNAMI, M., ISHIZAWA, A., WATANABE, T.-H. & SUGAMA, H. 2014 How to apply a turbulent transport model based on a gyrokinetic simulation for the ion temperature gradient mode in helical plasmas. *Journal of Physics: Conference Series* **561**, 012020.

Toda, S., Nunami, M., Murakami, S., Ishizawa, A., Watanabe, T.-H. & Sugama, H. 2015 Progress in applying gyrokinetic heat diffusivity model to transport simulations for helical plasmas. *20th International Stellarator-Heliotron Workshop, October, Greifswald, Germany,* P1S2-24 .

Watanabe, T.-H. & Sugama, H. 2006 Velocity–space structures of distribution function in toroidal ion temperature gradient turbulence. *Nucl. Fusion* **46**, 24.

Watanabe, T.-H., Sugama, H. & Ferrando-Margalet, S. 2007 Gyrokinetic simulation of zonal flows and ion temperature gradient turbulence in helical systems. *Nucl. Fusion* **47**, 1383.

Watanabe, T.-H., Sugama, H. & Ferrando-Margalet, S. 2008 Reduction of turbulent transport with zonal flows enhanced in helical systems. *Phys. Rev. Lett* **100**, 195002.

Xanthopoulos, P., Merz, F., Görler, T. & Jenko, F. 2007 Nonlinear gyrokinetic simulations of ion-temperature-gradient turbulence for the optimized Wendelstein 7-X stellarator. *Phys. Rev. Lett.* **99**, 035002.